Strain in Epitaxial Graphene Visualized by Intercalation

Stefan Schumacher,[1,*] Daniel F. Förster,[1] Malte Rösner,[2] Tim O. Wehling,[2,3] and Thomas Michely[1]

[1]*II. Physikalisches Institut, Universität zu Köln, Zülpicher Straße 77, 50937 Köln, Germany*

[2]*Institut für Theoretische Physik, Universität Bremen, Otto-Hahn-Allee 1, 28359 Bremen, Germany*

[3]*BCCMS, Universität Bremen, Am Fallturm 1a, 28359 Bremen, Germany*

(Received 11 July 2012; published 21 February 2013)

Intercalation of Eu under graphene on Ir(111) results in patterns oriented along the graphene moiré and quantized in size by its unit mesh. The patterns are formed by stripes, compact islands, and channels. Over a wide range of intercalated amounts the step concentration of the pattern has a rather constant saturation value. These findings are explained by the chemically modulated binding of graphene to the substrate and the preexisting strain in graphene due to its cooldown from the growth temperature. Local variations in the intercalation step density appear to reflect local variations in the preexisting strain.

DOI: 10.1103/PhysRevLett.110.086111 PACS numbers: 68.65.Pq, 68.35.Gy, 71.20.Tx, 81.16.Rf

Intercalation of gases, semiconductors, or metals in between an epitaxial graphene layer and its substrate has become an intensively studied topic. This strong interest is driven by the unique opportunities to decouple graphene (Gr) from its substrate, to perform or suppress chemistry under Gr, or to bestow it with entirely new properties.

Electronic decoupling of Gr from its substrate has been achieved, e.g., by intercalation of H underneath Gr on SiC(0001) [1]. This decoupling is utilized for an enhanced device performance [2]. Chemical decoupling and thereby exfoliation of epitaxial Gr was realized by bromine intercalation [3,4]. The confined space underneath Gr on Ru(0001) or Pt(111) is considered as a suitable container for reactions at sufficiently high temperatures [5–7]. At the same time Gr was shown to protect an intercalated Fe layer against oxidation [8]. Finally, a spin-orbit split Dirac cone was measured in Gr resting on an intercalated Au layer on Ni(111) [9]. Gr with a spin split Dirac cone together with its excellent spin transport properties opens the possibility for efficient spin filtering [10].

Motivated by the large Eu moment of $7\mu_B$, the coupling of these moments observed in the EuC_6 intercalation compound [11], and the ionic binding of Eu to Gr [12] leaving Gr's band structure intact, we investigated intercalation of Eu under epitaxial Gr on Ir(111) (Gr/Ir). We find a surprisingly rich and complex pattern formation of the Eu intercalation system, which is reported here.

We discuss, in the sequence given, three properties of Gr/Ir decisive for pattern formation. (i) The binding within the moiré unit cell is inhomogeneous resulting from the superposition of the Gr and Ir(111) lattices [13]. (ii) Intercalation affects the strain state of Gr. (iii) At ambient conditions Gr is under compressive strain due to the shrinkage of the substrate during the cooldown from the growth temperature [14,15]. The three properties are present for Gr on a large variety of epitaxial substrates and we therefore assume similar pattern formation processes to also exist for other systems. Although pattern formation by intercalation has not yet been reported for epitaxial Gr, indeed intercalation islands in sizes of multiples of the Gr moiré mesh [16–18] as well sharp intercalation fronts [5,6,19] were reported. We also point out that compared to the intercalation pattern described here, in a two phase system with competing short range attractive and long range repulsive interactions [20,21] the observability of stripes and islands in dependence of relative phase areas is reversed due to the different formation mechanism.

Experiments were performed in an ultrahigh vacuum variable temperature scanning tunneling microscopy (STM) system with a base pressure below 3×10^{-11} mbar. Ir(111) was prepared by cycles of sputtering at 920 K and annealing to 1520 K, yielding clean terraces with sizes in the order of 100 nm. A well oriented, coherent, and closed Gr monolayer was prepared by room temperature ethylene adsorption till saturation, thermal decomposition at 1500 K, and subsequent exposure to 5×10^{-7} mbar of ethylene at 1170 K for 600 s (TPG + CVD method) [22]. High purity Eu [23] was evaporated from a water cooled Knudsen cell in a background below 1×10^{-10} mbar with a flux of 3.5×10^{16} atoms m^{-2} s^{-1} while the sample was kept at 720 K during cooldown from the Gr growth temperature. Intercalated Eu amounts θ are specified in monolayers (ML), where $\theta = 1$ ML (or 100% ML) corresponds to a full (2×2) intercalation layer with respect to the Gr lattice. Imaging was conducted at room temperature if not specified otherwise. Typical parameters are $U_s \approx -1$ V for the sample bias and $I_t \leq 100$ pA for the tunneling current. The images were digitally postprocessed with the WSXM software [24].

Figures 1(a)–1(d) display the evolution of the surface pattern upon increasing exposure times of Gr/Ir to Eu at 720 K. Through Eu exposure elevations form that possess an apparent height of 1.5–2.5 Å, depending on the tunneling resistance. For all exposures, the elevations display rather sharp and straight edges that are oriented in directions with angles of 120° with respect to each other. For the

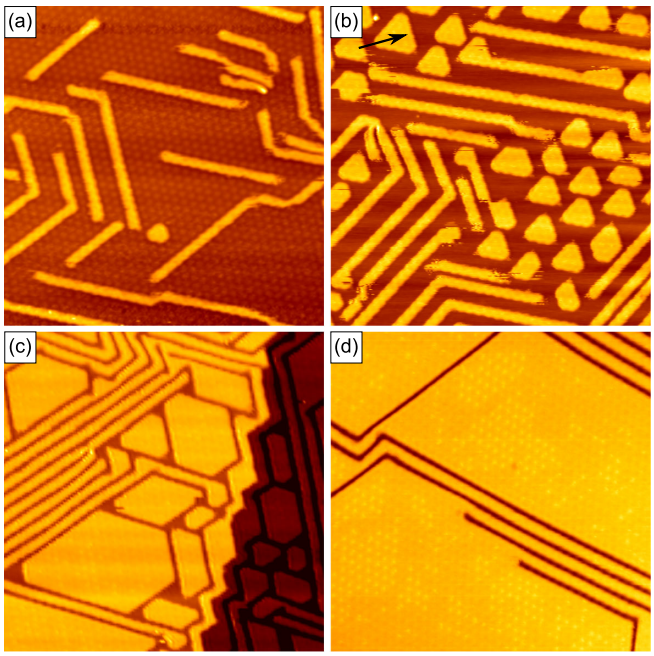

FIG. 1 (color online). (a)–(d) STM topographs (image size 80 nm × 80 nm) after intercalation of Eu resulting in successively larger intercalation coverages of (a) 18% ML, (b) 39% ML, (c) 72% ML, and (d) 89% ML. The arrow in (b) indicates the [$\bar{1}\,\bar{1}\,2$] direction.

smallest Eu exposure (coverage 18% ML) in Fig. 1(a), the deposited Eu causes the formation of thin stripes (*t* stripes). The *t* stripes have a width of 2.35 ± 0.15 nm measured at half height. The standard deviation specifies the spread, not the much smaller error. At a coverage of 39% ML as shown in Fig. 1(b) *t* stripes are complemented by compact islands. The islands have a preference for a triangular shape with one tip pointing upward. The symmetry of the morphology is thus only threefold and not sixfold. At a coverage of 72% ML as shown in Fig. 1(c) a tendency of the *t* stripes to form bundles with a periodicity of 3.75 ± 0.15 nm is visible. Besides bundles large compact islands of irregular hexagonal shape and wider stripes are also visible. All pattern elements are separated by strait channels (*s* channels) with a width of 1.4 ± 0.1 nm at half height. Finally, close to layer completion (coverage 89% ML) as shown in Fig. 1(d) the islands have become large and the number of *s* channels has decreased. Still, even for this large coverage *t*-stripe bundles are present. Fluctuations of the morphology with time indicate that the system is close to equilibrium [25].

Low energy electron diffraction (LEED) and atomic resolution STM imaging at low temperature provided in Ref. [25] prove that Eu intercalates in a (2 × 2) superstructure with respect to Gr. Density functional theory calculations as specified in Refs. [12,25] confirm that the (2 × 2)-Eu superstructure is the lowest energy configuration for Gr/Eu/Ir with a binding energy of −3.8 eV/Eu atom. In contrast, Eu/Gr/Ir in the same superstructure is bound only by −1.4 eV/Eu atom. The large energy gain of 2.4 eV/atom drives the intercalation process. Nevertheless, for a perfect Gr layer the Eu intercalation is an activated process and requires elevated temperatures well above 300 K [12].

In Figs. 1(a) and 2(a) a hexagonal lattice of bright protrusions with a separation of $a_m = 2.53$ nm is visible between intercalation islands and *t* stripes. This lattice (and not the atomic Gr lattice [25]) defines the positioning of the intercalated objects. Islands and stripes display straight edges with respect to this lattice and grow in multiples of bright protrusion distances; i.e., they are quantized in units of a_m. The bright protrusions mark the periodicity a_m of the moiré formed by Ir(111) with Gr. The moiré mesh consists of 10.32 × 10.32 Gr unit cells resting on 9.32 × 9.32 Ir atoms [26]. Because of the varying lateral positioning of the C atoms with respect to Ir, we identify three high symmetry configurations: in an atop area (fcc and hcp area) we find underneath the center of a hexagonal C ring an atop Ir site (regular hollow or fcc site and faulted hollow or hcp site). In Fig. 2(a) we tiled the moiré cell schematically by white, green, and red hexagons, representing atop, fcc, and hcp areas, respectively (for identification of the areas see Ref. [25]).

In Fig. 2(b) the morphology of Fig. 2(a) is redrawn into the tiled moiré pattern, with the boundaries of the intercalation islands and *t* stripes following schematically the boundaries between tiles. The thinnest intercalation object, the *t* stripe incorporates two rows of white tiles (atop areas) and one row of red and green tiles each; stripes wider by *N* moiré unit cells incorporate *N* additional rows of each color. All boundaries of intercalation objects, as well as *s* channels, are formed by red and green tiles without any white tiles. Finally we note that the two edges of a *t* stripe are not equivalent: One edge is predominantly bounded by red tiles (*r* edge), the other one by green tiles (*g* edge). Comparison with Fig. 1(b) shows that the

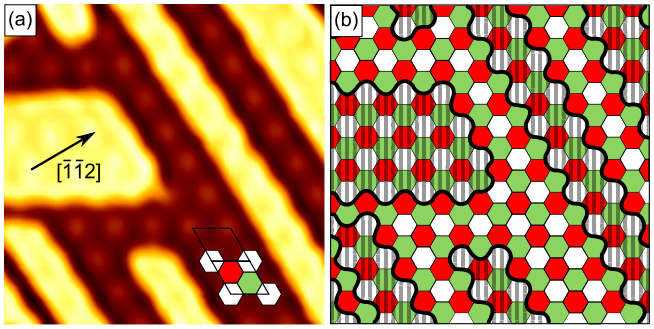

FIG. 2 (color online). (a) STM topograph (21 nm × 21 nm) after intercalation of 50% ML Eu at 720 K. Based on the different local symmetries of C rings with respect to the substrate, the moiré unit cell (black rhomboid) is tiled. White: atop area; green (light gray): fcc area; red (dark gray): hcp area (see text). The arrow indicates the Ir[$\bar{1}\,\bar{1}\,2$] direction. (b) Schematic sketch of (a) redrawn into the tiled moiré pattern.

triangular intercalation islands are predominantly bounded by r edges. The inequivalence of the two edges thus explains the only-threefold pattern symmetry. Further evidence for the inequivalence of r and g edges can be found by low temperature imaging of the intercalated patterns [25].

In Ref. [13] it was found that the binding of Gr to Ir is largely physisorption with an average binding energy per C atom of -50 meV. However, this binding is modulated with weak chemical bonds in the fcc and hcp areas and chemical repulsion in the atop areas. It appears thus that t stripes are a preferred morphological entity just for their high fraction of delaminated atop areas. For the same reason the tiles energetically most costly to delaminate accumulate in the remaining nonintercalated areas, for instance as s channels. As intercalated islands are preferentially bounded by r edges, it is plausible that hcp areas are even more strongly bound than fcc ones.

It is tempting to attribute the intercalation pattern to the binding inhomogeneity of the Gr moiré. Based on the analysis above, we assume that the delamination energy per C atom in the atop area E_{atop} is substantially smaller than the corresponding energies E_{fcc} and E_{hcp} in the fcc and hcp areas. The monotonic decrease of the fraction of white tiles with increasing stripe width from $1/2$ for a t stripe via $3/7$ for a $(t+1)$ stripe to $1/3$ in the limit of very wide stripes, in combination with the width of a t stripe being greater than a moiré unit cell, suggests that the intercalation energy cost per Eu atom E_{in} is monotonically increasing with stripe width: $E_{\mathrm{in}}(t) < E_{\mathrm{in}}(t+1) < E_{\mathrm{in}}(t+N)$ with N larger than 1. A quantitative analysis for a one-dimensional stripe situation [25] shows that the delicate balance of E_{atop}, E_{edge}, and the width x available in a t stripe for intercalation determines, whether $E_{\mathrm{in}}(t+N)$ is a monotonically increasing and concave function of N (t stripes energetically preferred) or a monotonically decreasing and convex function of N (a single island with large N preferred). With the reasonable assumptions $E_{\mathrm{atop}} = 0$ eV, $E_{\mathrm{edge}} = 0$ eV, and $x = 5.5$ Eu rows in a t stripe we obtain a preference by about 0.7 eV per moiré unit cell to accommodate Eu in t stripes compared to a single island.

The energetic preference of t stripes predicts a linear growth of the intercalation step density ρ with θ until the entire surface is covered with t stripes at $\rho = 0.27$ nm^{-1} (compare Fig. 3, blue solid line). Increasing the coverage further causes a linear decrease of ρ until it vanishes for full coverage. A quantitative analysis of the experimentally observed intercalation step density ρ as a function of θ is also presented in Fig. 3. ρ is obtained by counting steps along a grid of orthogonal lines in areas free of preexisting substrate steps. Still the scatter of ρ is substantial. Nevertheless, it is obvious that beginning with small θ, a rapid increase of ρ takes place, then for 30% ML $< \theta <$ 80% ML a broad plateau with $\rho = 0.09$–0.12 nm^{-1} is reached and finally ρ decreases again rapidly to zero. While the observed ρ for small and large θ agrees reasonably well with our expectations, the broad plateau is inconsistent with the assumption that the intercalation pattern is only driven by the chemical inhomogeneity of binding in the moiré.

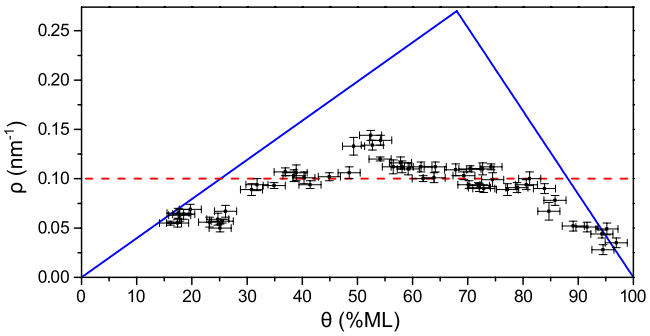

FIG. 3 (color online). Intercalation step density ρ as a function of intercalated Eu amount θ. Blue solid line: expected $\rho(\theta)$ if t stripes are energetically preferred (no strain). Red dashed line: expected $\rho(\theta)$ taking only strain relaxation of Gr into account (no binding inhomogeneity and edge energy).

Therefore, we need to take a close look at other changes in the surface energetics associated with intercalation. Figure 4 displays a single t stripe with the surrounding moiré well resolved. The height profile along the blue line shows a rather regular spacing of the depressions of $\sqrt{3}a_m = 4.38$ nm. The t stripe gives rise to a lateral shift of the moiré by $\Delta s_m = 0.33$ nm. This shift is due to the arc length increase of Gr bending over the t stripe. The corresponding lateral shift of the C atoms in Gr is $\Delta s_t = 0.032$ nm, which is obtained from Δs_m using standard moiré methods [27]. Averaging of similar situations results in $\Delta s_t = 0.037 \pm 0.005$ nm for single stripes [28]. For stripe bundles

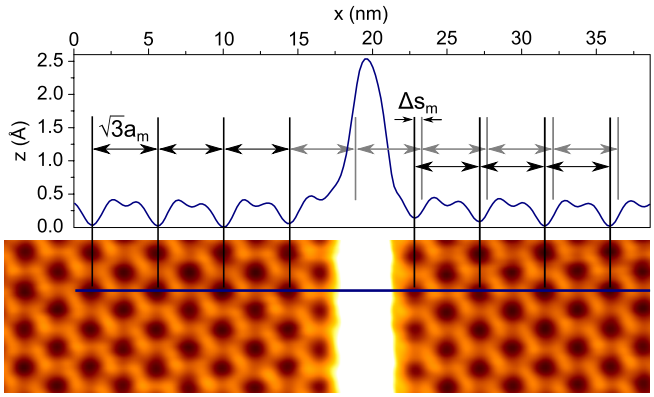

FIG. 4 (color online). Height profile over a single t stripe taken along the blue line in the STM image (43 nm × 10 nm). The moiré periodicity of $\sqrt{3}a_m$ in path direction is displaced by Δs_m due to the t stripe (see text). Because of the inverted moiré contrast atop areas are imaged now as dark spots. The imaging contrast (regular or inverted) depends on tip state and tunneling resistance [26].

we obtain a significantly larger arc length increase of $\Delta s_{t,b} = 0.060 \pm 0.012$ nm per stripe. Here $\pm$ again denotes the standard deviation of the scatter. Obviously, intercalation pattern formation is associated with a change of the strain state in Gr.

The CVD growth step of the Gr/Ir used here is conducted at 1170 K. Due to the mismatch of the thermal expansion coefficients of Gr and Ir a compressive strain of $\epsilon = 0.6\%$ in Gr results upon cooling to room temperature if strain relaxation is absent. Without intercalation a significant part of the strain relaxes by nucleation of wrinkles 400 K below the growth temperature leaving a residual compressive strain of 0.3% at ambient temperature [14,15]. After intercalation we rarely find wrinkles on the sample. It is therefore plausible that most of the 0.6% thermal mismatch strain is released by intercalation via formation of intercalation steps.

Starting with a Gr surface compressively strained by $\epsilon = 0.6\%$, formation of a first stripe with two intercalation steps will release an elastic energy per length a_m of $\Delta E = Y n a_m \epsilon \Delta s_t$. Here Y denotes Young's modulus (56 eV per C atom) and n the density of C atoms (38.2 nm^{-2}). Using $\Delta s_t = 0.037$ nm we arrive at a sizable energy gain of 1.2 eV. Upon formation of more stripes the energy gain will decrease until for $\rho = 0.1$ nm^{-1} the Gr is entirely relaxed as indicated by the dashed line in Fig. 3 (compare Ref. [25] for quantitative analysis). If a few wrinkles are still present after intercalation—a situation we can not exclude—the dashed line in Fig. 3 is just shifted to somewhat smaller values. Preexisting strain and its relaxation through intercalation steps yields a simple explanation for the broad plateau in ρ for intermediate coverages. After complete strain relaxation additional intercalation would drive Gr into a tensile state with the buildup of new strain energy. Formation of additional t stripes—instead of growing existing ones wider—therefore ceases when the associated tensile strain energy becomes larger than the energetic advantage of t-stripe formation due to the binding energy inhomogeneity.

Relaxation of preexisting compressive strain in Gr *alone* is unable to explain the observed patterns. One would expect the formation of stripes (channels) even thinner than the t stripes (s channels) for very small (very large) θ to achieve a maximum in strain relaxation, contrary to observation.

Our simple view of intercalation pattern formation provides a natural explanation for the inhomogeneous distribution of intercalation steps over the sample, specifically near steps. Since ρ is defined by a situation where the preference for t-stripe formation is balanced by a buildup of tensile strain, the local variation of ρ reflects initial variations in the distribution of preexisting compressive strain. The examples visualized by Fig. 5 support this view. In Fig. 5(a) an unusually high intercalation step density realized by t-stripe bundles is visible on the terrace near a concave substrate step, which shortly merges with a second one to a double step (large initial Gr compression). In contrast, ρ is low on the terrace next to the descending convex substrate step (strain was released by the Gr moving out). Similarly, for a Gr band next to a substrate step [Fig. 5(b), only partial Gr coverage] the s channels are normal to the long axis of the band, where strain relaxation could not be achieved during cooldown.

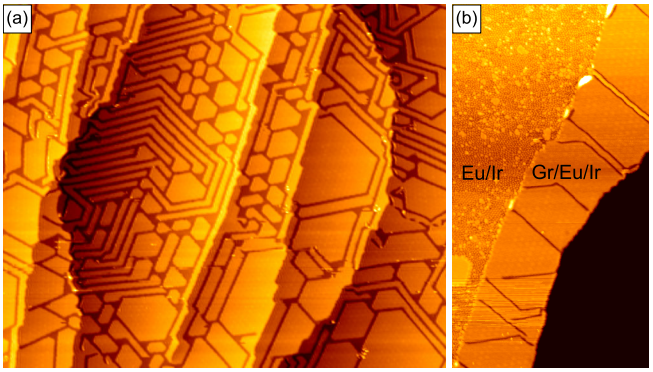

FIG. 5 (color online). (a) STM topograph (195 nm × 160 nm) after intercalation of 72% ML Eu. (b) STM topograph (70 nm × 130 nm) after Eu deposition on Ir(111) covered with 40% ML Gr.

The question remains why the strain relief pattern is dominated by one-dimensional stripes for small and large intercalated amounts, although Gr should be isotropically strained. Such a spontaneous symmetry break was also observed for the herringbone reconstruction of Au (111) and linked to long range substrate mediated elastic interactions [29]. In our case, more isotropic pattern elements than t stripes with a comparable delamination energy per Eu atom (same fraction of white tiles) are probably unfavored due to higher costs for Gr bending contributing to the edge energy.

In conclusion, pattern formation upon Eu intercalation underneath Gr on Ir(111) can consistently be explained by the interplay of the moiré binding inhomogeneity and a change in the strain state of Gr due to intercalation. For intermediate intercalated amounts the local variation in intercalation step density reflects and visualizes the local variations in the initial strain distribution.

The authors acknowledge financial support through Deutsche Forschungsgemeinschaft via SFB608 and Project No. MI581/17-2 as well as useful discussions with Carsten Busse and Achim Rosch.

*sschumacher@ph2.uni-koeln.de

[1] C. Riedl, C. Coletti, T. Iwasaki, A. A. Zakharov, and U. Starke, Phys. Rev. Lett. **103**, 246804 (2009).
[2] J. A. Robinson, M. Hollander, M. LaBella, K. A. Trumbull, R. Cavalero, and D. W. Synder, Nano Lett. **11**, 3875 (2011).

[3] E. Widenkvist, D. W. Boukhalov, S. Rubino, S. Akhtar, J. Lu, R. A. Quinlan, M. I. Katsnelson, K. Leifer, H. Grennberg, and U. Jansson, J. Phys. D **42**, 112003 (2009).
[4] C. Herbig, M. Kaiser, N. Bendiab, S. Schumacher, D. F. Förster, J. Coraux, K. Meerholz, T. Michely, and C. Busse, J. Phys. Condens. Matter **24**, 314208 (2012).
[5] P. Sutter, J. T. Sadowski, and E. A. Sutter, J. Am. Chem. Soc. **132**, 8175 (2010).
[6] E. Starodub, N. C. Bartelt, and K. F. McCarty, J. Phys. Chem. C **114**, 5134 (2010).
[7] R. Mu, Q. Fu, L. Jin, L. Yu, G. Fang, D. Tan, and X. Bao, Angew. Chem., Int. Ed. **51**, 4856 (2012).
[8] Y. S. Dedkov, M. Fonin, U. Rüdiger, and C. Laubschat, Appl. Phys. Lett. **93**, 022509 (2008).
[9] A. Varykhalov, J. Sánchez-Barriga, A. M. Shikin, C. Biswas, E. Vescovo, A. Rybkin, D. Marchenko, and O. Rader, Phys. Rev. Lett. **101**, 157601 (2008).
[10] H. Haugen, D. Huertas-Hernando, and A. Brataas, Phys. Rev. B **77**, 115406 (2008).
[11] G. Kaindl, J. Feldhaus, U. Ladewig, and K. H. Frank, Phys. Rev. Lett. **50**, 123 (1983).
[12] D. F. Förster, T. O. Wehling, S. Schumacher, A. Rosch, and T. Michely, New J. Phys. **14**, 023022 (2012).
[13] C. Busse, P. Lazić, R. Djemour, J. Coraux, T. Gerber, N. Atodiresei, V. Caciuc, R. Brako, A. T. N'Diaye, S. Blügel, J. Zegenhagen, and T. Michely, Phys. Rev. Lett. **107**, 036101 (2011).
[14] A. T. N'Diaye, R. van Gastel, A. J. Martínez-Galera, J. Coraux, H. Hattab, D. Wall, F.-J. Meyer zu Heringdorf, M. Horn-von Hoegen, J. M. Gómez-Rodríguez, B. Poelsema, C. Busse, and T. Michely, New J. Phys. **11**, 113056 (2009).
[15] H. Hattab, A. T. N'Diaye, D. Wall, C. Klein, G. Jnawali, J. Coraux, C. Busse, R. van Gastel, B. Poelsema, T. Michely, F.-J. Meyer zu Heringdorf, and M. Horn-von Hoegen, Nano Lett. **12**, 678 (2012).
[16] H. Zhang, Q. Fu, Y. Cui, D. Tan, and X. Bao, J. Phys. Chem. C **113**, 8296 (2009).
[17] S. Forti, K. V. Emtsev, C. Coletti, A. A. Zakharov, C. Riedl, and U. Starke, Phys. Rev. B **84**, 125449 (2011).
[18] M. Sicot, P. Leicht, A. Zusan, S. Bouvron, O. Zander, M. Weser, Y. S. Dedkov, K. Horn, and M. Fonin, ACS Nano **6**, 151 (2012).
[19] K. V. Emtsev, A. A. Zakharov, C. Coletti, S. Forti, and U. Starke, Phys. Rev. B **84**, 125423 (2011).
[20] K.-O. Ng and D. Vanderbilt, Phys. Rev. B **52**, 2177 (1995).
[21] R. Plass, J. A. Last, N. C. Bartelt, and G. L. Kellogg, Nature (London) **412**, 875 (2001).
[22] R. van Gastel, A. T. N'Diaye, D. Wall, J. Coraux, C. Busse, N. M. Buckanie, F.-J. Meyer zu Heringdorf, M. Horn-von Hoegen, T. Michely, and B. Poelsema, Appl. Phys. Lett. **95**, 121901 (2009).
[23] High purity Eu was obtained from Ames Laboratory (Materials Preparation Center) of the US DOE, Iowa State University, Ames, Iowa 50011-3020, USA.
[24] I. Horcas, R. Fernández, J. M. Gómez-Rodríguez, J. Colchero, J. Gómez-Herrero, and A. M. Baro, Rev. Sci. Instrum. **78**, 013705 (2007).
[25] See Supplemental Material at http://link.aps.org/supplemental/10.1103/PhysRevLett.110.086111 for a more detailed description of the pattern structure and orientation, density functional theory calculations, and intercalation energetics.
[26] A. T. N'Diaye, J. Coraux, T. N. Plasa, C. Busse, and T. Michely, New J. Phys. **10**, 043033 (2008).
[27] J. Coraux, A. T. N'Diaye, C. Busse, and T. Michely, Nano Lett. **8**, 565 (2008).
[28] The tiling of Fig. 2(b) only approximates the final situation after intercalation to an accuracy ignoring Δs_m. However, the tiling of Fig. 2(b) represents exactly the areas to be delaminated upon intercalation.
[29] S. Narasimhan and D. Vanderbilt, Phys. Rev. Lett. **69**, 1564 (1992).